Nature of phosphorus embrittlement of the FeΣ3[1$\bar{1}$0](111) grain boundary

Ruqian Wu and A. J. Freeman
Department of Physics & Astronomy, Northwestern University, Evanston, Illinois 60208

G. B. Olson
Department of Materials Science and Engineering, Northwestern University, Evanston, Illinois 60208
(Received 10 January 1994; revised manuscript received 4 April 1994)

Thermodynamic, electronic, and magnetic properties of the P/FeΣ3[1$\bar{1}$0](111) grain boundary and the P/Fe(111) free surface are compared using the full potential linearized augmented plane-wave method. The calculated segregation-energy difference of 0.8 eV is consistent with the embrittling effect of P according to the Rice-Wang thermodynamic model. The clean FeΣ3[1$\bar{1}$0](111) boundary is found to undergo an ω phase transition which results in an antiferromagnetic coupling within the core of the grain boundary. Structural relaxations in the grain boundary alter the P segregation energy by ~2.0 eV and are found to play an important role in defining the correct sign and value of the segregation energy difference controlling embrittlement. The P/Fe chemical interaction is found to be "embeddedlike" electrostatic rather than covalent in both environments. Long-range effects of P impurities are found for the Fe magnetization which reduce the embrittling potency of P.

I. INTRODUCTION

Advances in the present state-of-the-art total-energy electronic structure calculational techniques and computational facilities, together with a new level of understanding of the atomic structure of grain boundaries, make it possible to approach the mechanisms of intergranular embrittlement at a more fundamental level than ever before possible.[1] The potential for a predictive theory of intergranular cohesion, coupled with a new level of microstructural control allowed by novel techniques such as rapid solidification processes, offers promise of major improvements in grain boundary (GB) sensitive properties such as the stress corrosion resistance of ultrahigh strength steels.

A thermodynamic theory developed by Rice and coworkers[2,3] describes the mechanism of metalloid-induced intergranular embrittlement through the competition between dislocation crack blunting vs brittle separation. While crystal plasticity considerations show interesting directional effects on the relative ease of dislocation emission from the crack tip, as tested in critical bicrystal experiments,[4] the most striking result of the analysis is the prediction that the potency of a segregating solute in reducing the "Griffith work" of brittle boundary separation is a linear function of the difference in segregation free energy for that solute at a grain boundary Δg_b^0 and a free surface (FS) Δg_s^0 (or similarly the difference between segregation energies ΔE_b^0 and ΔE_s^0, since segregation entropies are relatively small). Simply put, a solute with a positive energy difference $\Delta g_b^0 - \Delta g_s^0$ (i.e., Δg_b^0 is less negative) will be a more potent embrittler, or vice versa.

The validity of this hypothesis has been supported experimentally for Fe-base materials for which the greatest amount of data exists for both the relative embrittling potencies of solutes and the relevant surface thermodynamic quantities.[1] Therefore, we can explore the embrittlement problem using present state-of-the-art energy band theory from the point of view of total-energy differences for GB and FS systems. To this end, we previously carried out full potential linearized augmented plane-wave (FLAPW) total-energy calculations to investigate the effects of a phosphorus impurity in the FeΣ3[1$\bar{1}$0](111) grain boundary and on the corresponding Fe(111) surface.[5] With a cell that only contained the first neighbor Fe atoms to the P impurity, we found that the Fe-P chemical bonding is stronger at the Fe(111) surface due to a shorter interatomic distance. However, the calculated $\Delta E_b^0 - \Delta E_s^0$ was negative (−1.1 eV/cell), in contrast to the observation that P is an embrittler for Fe cohesion. This discrepancy was attributed to (i) the small cell size used and (ii) the exclusion of atomic structural relaxation. Indeed, according to our more recent DMol cluster calculations,[6] the atomic structures for the FeΣ3[1$\bar{1}$0](111) GB differ significantly with and without the presence of the P impurity. This structural relaxation may reduce the total energy of the clean FeΣ3[1$\bar{1}$0](111) GB (i.e., the reference system for ΔE_b^0) by an amount as large as 2 eV/cell which, in turn, results in the same amount of overestimation for ΔE_b^0. By contrast, the impurity atoms do not induce significant reconstruction for the Fe(111) surface (due to the large free space on the vacuum side).[7] Therefore, the inclusion of the impurity-induced relaxation in the GB is very important for defining $\Delta E_b^0 - \Delta E_s^0$.

In the present paper, we extend our studies for the P/Fe system by (i) expanding the size of unit cell and (ii) including the atomic structural relaxation for both the GB and FS. Following presentation of the model and computational details in Sec. II, we discuss the ω phase

transition and its effects on the electronic and magnetic properties for the clean FeΣ3[1$\bar{1}$0](111) GB in Sec. III. The basis of the P-induced intergranular embrittlement for the Fe grain boundary is developed in Sec. IV from considerations of chemical bonding, magnetic properties, and total-energy differences between the grain boundary and FS systems. Finally, concluding remarks are given in Sec. V.

II. MODEL AND COMPUTATION

Since the final results for $\Delta E_b^0 - \Delta E_s^0$ are very small (one order smaller than either ΔE_b^0 or ΔE_s^0), it is very important to treat the surface and the GB systems equally. Therefore, as sketched in Fig. 1, we used a slab model to simulate both the P/FeΣ3[1$\bar{1}$0](111) GB and P/Fe(111) FS. The two-dimensional (2D) lattice constant and the unrelaxed interatomic Fe-Fe distance are chosen from experiment ($d_{\text{Fe-Fe}}$=4.69 a.u.). For FS systems, a 13-layer slab is adopted for the Fe(111) substrate so as to eliminate possible size effects (i.e., the remaining interaction between the two surfaces on both sides of the slab). For the same reason, we use a 23-layer slab to simulate the clean FeΣ3[1$\bar{1}$0](111) GB. With 12 Fe layers in between, the influence of the surface (introduced artificially in the slab model) on the grain boundary properties is expected to be sufficiently small. We avoid the strong lattice stress inherent at the hypothetical unit cell boundary in previous superlattice model calculations.[5,8] In addition, systematic error cancellations are expected for $\Delta E_b^0 - \Delta E_s^0$ by using the slab model for both the surface and GB with the same set of k points and the same basis functions.

With sufficiently thick slab models, it is feasible to take multilayer atomic relaxation into account for Fe in both GB and surface environments. For the clean and P-adsorbed Fe(111) surface, the equilibrium atomic geometry is determined through FLAPW total-energy minimization.[5,7,9] For the grain boundary case, geometries obtained from DMol cluster atomic force calculations[6] are adopted.

In the FLAPW method,[10] no shape approximations are made to the charge densities, potentials, and matrix elements. The core states are treated fully relativistically and the valence states are treated semirelativistically (i.e., without spin-orbit coupling).[11] We employ the Hedin-Lundqvist and the von Barth–Hedin formulas for the exchange-correlation potentials for the nonmagnetic (NM) and the spin-polarized calculations, respectively.[12] This approach has been applied very successfully in the last decade to determine the structural, electronic, and magnetic properties of many transition metal systems.[13]

Energy cutoffs of 11 Ry and 70 Ry are employed for the plane-wave bases and star functions to describe the wave function and both the charge density and potential in the interstitial region, respectively. Within the muffin-tin (MT) spheres ($r_{\text{MT,Fe}} = 2.0$ a.u., $r_{\text{MT,P}} = 1.8$ a.u.), lattice harmonics with angular momentum l up to 8 are adopted. Convergence is assumed when the average root-square difference between the input and output charge (spin) densities is less than 5×10^{-4} $e/(\text{a.u.})^3$ (1×10^{-4} $e/(a.u.)^3$). The step-forward fixed-basis approach, which was originally designed for massive parallelization purposes,[14] is used to speed up the calculations by a factor of 3.

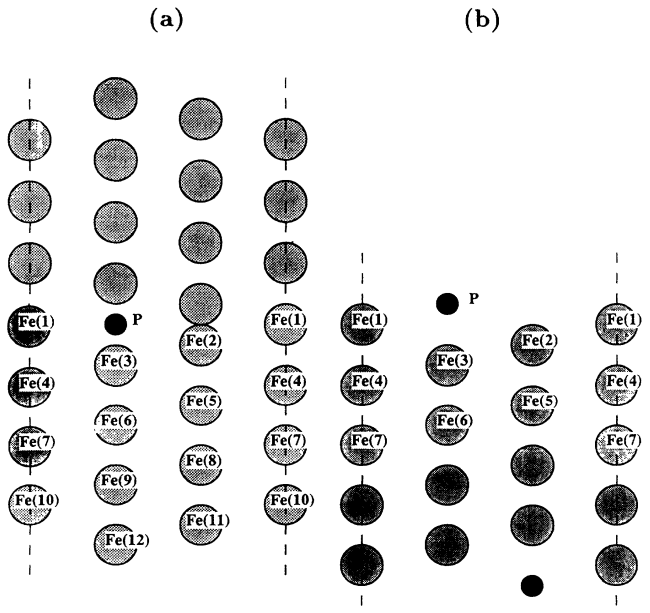

FIG. 1. Model and notation for the structure of (a) the P/Fe Σ3[1$\bar{1}$0](111) "incoherent" twin boundary and (b) the P/Fe(111) surface.

III. STRUCTURAL RELAXATION OF THE CLEAN GRAIN BOUNDARY

For the unrelaxed FeΣ3[1$\bar{1}$0](111) GB starting from a coincident-site configuration, there is a high repulsion between the two Fe(2) atoms across the grain boundary. Both DMol cluster[6] and embedded atom method[15] calculations revealed that the clean FeΣ3[1$\bar{1}$0](111) GB undergoes a comprehensive long-range structural relaxation. The most important feature is that, at equilibrium, the Fe(2) and Fe(3) atoms [also Fe(5) and Fe(6) atoms] merge into almost the same plane, forming a closely packed hexagonal Fe layer structure analogous to the ω phase observed in Ti alloys. This phase transition at the clean FeΣ3[1$\bar{1}$0](111) GB is expected to affect the electronic and magnetic properties drastically.

In Fig. 2(a), the calculated charge density is presented on a vertical (1$\bar{1}$0) plane for the clean FeΣ3[1$\bar{1}$0](111) GB. Obviously, the profile of contours in the core region of the GB differ substantially from those around the Fe(9) atom, where a typical bulk character is reproduced. Here the interatomic distance between Fe(2) and Fe(3), 4.42 a.u., contracts by 6% from that in bcc bulk Fe, 4.69 a.u., while the Fe(1)-Fe(2,3) interatomic distance increases to 5.01 a.u. Consequently, as shown by the charge density contours in Fig. 2(a), the Fe-Fe intraplane interaction becomes much stronger than the interplane one, which is expected to introduce some unique features for "ω" Fe.

Indeed, as shown by the spin density in Fig. 2(b),

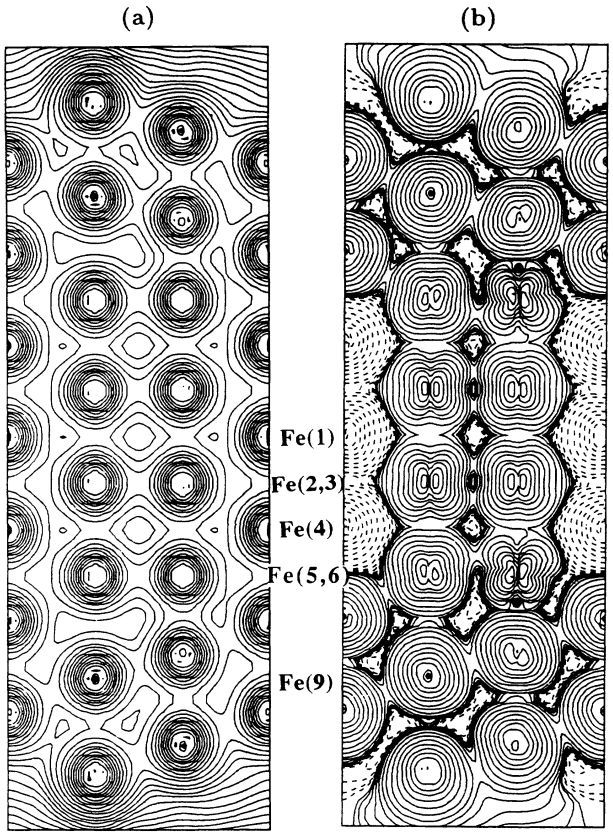

FIG. 2. The calculated (a) valence charge density and (b) spin density of the clean FeΣ3[1$\bar{1}$0] (111) grain boundary. Contours in panel (a) start from 1×10^{-4} e/a.u.^{3} and increase successively by a factor of $\sqrt{2}$, and in panel (b) start from $\pm 1 \times 10^{-4}$ e/a.u.^{3} and vary successively by a factor of 2. Dashed lines in panel (b) indicate negative spin density.

an interplane antiferromagnetic (AFM) coupling can be found in the core region of the grain boundary. Since this AFM state was obtained from a preassigned ferromagnetic (FM) state (with a large moment of $3\mu_B$/atom) through self-consistent iterations, we believe that the AFM state is a stable ground state for the ω FeΣ3[1$\bar{1}$0](111) GB (the FM state may exist as a metastable state with a much higher energy). At the coherent interface between the ω and the bcc Fe, the contracted Fe(5)-Fe(8) interatomic distance (4.16 a.u.) supresses markedly the spin polarization around the Fe(5) atom. Quantitatively, as listed in Table I (in the column for GB0), the Fe(5) magnetic moment is only $0.8\mu_B$, about one-third that in bcc Fe ($2.22\mu_B$). Suppressed by either the smaller interatomic distance (and hence stronger chemical interaction) or the AFM coupling, the magnetic moments are smaller than $2.2\mu_B$ for almost all Fe atoms. Interestingly, for Fe(1) and Fe(4), the valence and core contributions to the Fermi contact hyperfine field almost completely cancel each other, resulting in a small net Fermi contact hyperfine field ($\sim$ 10 kG), which may provide a way to experimentally verify the predicted ω phase transition and thus induced AFM coupling in the clean FeΣ3[1$\bar{1}$0](111) GB.

TABLE I. Calculated magnetic moments (in μ_B) in Fe. GB0 and GB1 represent the relaxed and unrelaxed clean Fe GB configurations, respectively, obtained after removing the P from the P/Fe system.

Atom	Fe GB0	Fe GB1	P/Fe GB	Fe(111)	P/Fe(111)
Fe(1)	−1.28	2.40	1.40	2.71	1.74
Fe(2)	1.56	2.11	1.81	2.29	2.22
Fe(3)	1.43	1.81	1.49	2.36	1.73
Fe(4)	−1.75	1.81	2.01	2.20	2.30
Fe(5)	0.80	2.10	2.05	2.20	2.17
Fe(6)	1.42	1.85	1.98	2.11	2.27
Fe(7)	1.68	2.10	2.14	2.02	2.24

IV. EFFECTS OF THE PHOSPHORUS IMPURITY

A. Atomic structure

For the P/FeΣ3[1$\bar{1}$0](111) GB, DMol calculations carried out for a 92-atom cluster[6] showed that P impurities induce a strong atomic reconstruction for Fe atoms from their positions in the ω phase. While the close-packed vertical Fe(2) chain remains almost unaffected, the two Fe(3) atoms across the GB are pushed apart by 4.15 a.u. The calculated P-Fe(3) bond length, 4.42 a.u.,[6] is 3% larger than the value measured from the Fe_3P compound, 4.27 a.u. (Ref. 16) (also assumed for the P-Fe GB in our previous small-cell calculations[5]). Consequently, Fe(6) and Fe(9) are also pushed away from the center GB plane by 1.70 a.u. and 0.76 a.u. with respect to their position in the clean FeΣ3[1$\bar{1}$0](111) GB.

On the clean Fe(111) surface, by contrast, the P adsorbate has room to adjust its position without strongly disturbing the substrate atoms. FLAPW calculations[9] predict that the clean Fe(111) surface undergoes a substantial multilayer relaxation due to its open structure. The calculated surface relaxation is 0.38 a.u. inward, in good agreement with experiment.[17] After adsorbing P atoms, the surface relaxation is almost fully recovered.[7] The calculated equilibrium P-Fe bond length is 4.05 a.u. in the P/Fe(111)-adsorption system, which is 8% shorter than that in the GB.

B. Chemical interaction

The charge redistribution for the P-segregated FeΣ3[1$\bar{1}$0](111) GB, obtained by substracting the superimposed charge density from a free P monolayer and a hypothetical unrelaxed clean Fe grain boundary (with the same atomic structure as that in the P-doped case) from the self-consistent charge density for the P/Fe GB, is presented in Fig. 3(a) together with the counterpart for the P/Fe(111) in Fig. 3(b). Charge accumulations are clearly shown in the region between P-Fe(3) and P-Fe(1), indicating some strong chemical interaction between these atoms. Noticeably, the charge density at the inner region around the P atom is decreased due to the effects of surrounding Fe atoms. This apparent reverse charge

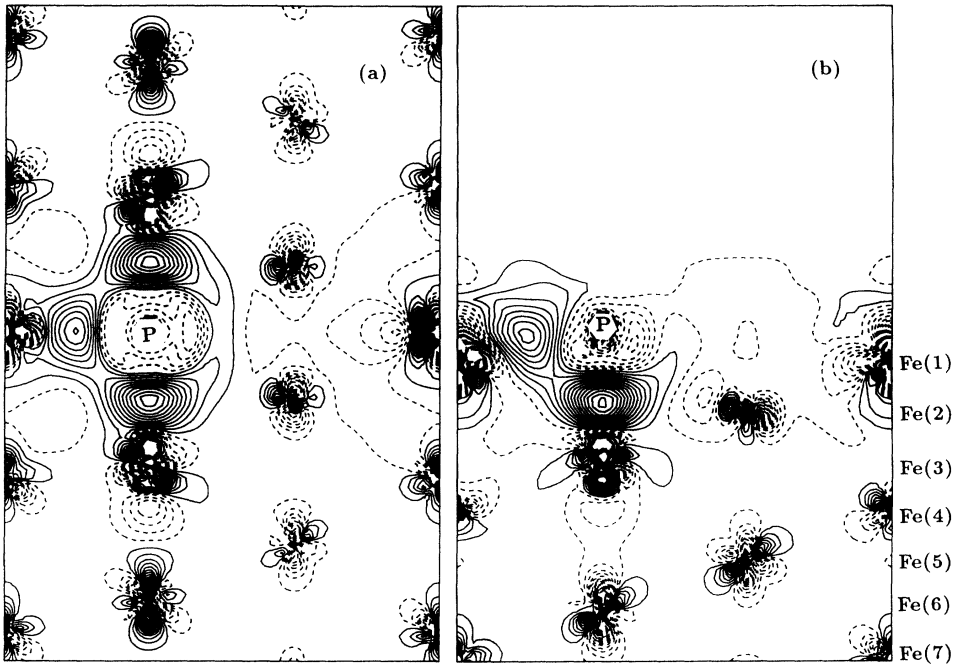

FIG. 3. The P-induced charge density difference for (a) P/FeΣ3[1$\bar{1}$0] (111) grain boundary and (b) P/Fe(111) free surface. Dashed lines show negative differences.

transfer contradicts the simple estimate from electronegativity (2.19 for P and 1.83 for Fe).

These behaviors can be understood, however, from the large spatial extension of the P-3p wave function, which forms a 3p band as wide as 3 eV for the free-standing P monolayer,[5] even though the P-P interatomic distance is 7.66 a.u. In Fig. 4, the contributions from the 3s and 3p states to the valence charge density of the free-standing P monolayer is presented along the P-Fe(3) direction. Clearly, due to the existence of the nodes, the main peaks of the 3s and 3p radial wave functions of the P atom lie almost outside of its potential well with long tails extending 4 a.u. away from the P nucleus. As a result, these wave functions are expected to be strongly affected by foreign atoms (i.e., soft wave function by contrast to the Fe 3d hard wave function, which lies mainly in its potential well and thus is hardly affected by environmental changes). In the GB, the potential is significantly lowered by the Fe(3) atom in the region 1.5 a.u. away from the P nucleus. The P 3p wave function will undergo distortion under the influence of two factors. First, P 3p electrons can directly feel the attraction from the Fe nuclei, which pull the P 3p wave function outerward and so result in a reduction of the weight at the inner lobe around the P atom. Second, the strong Coulomb and Pauli repulsions push P 3p electrons away from the high density region around the Fe atoms. The net action from these two effects is to squeeze the P 3p electrons into the intermediate region between P and Fe atoms. This mechanism of Fe-induced distortion for the metalloid wave function is similar to the concept of the embedded atom interacting via electrostatic potential instead of hybridization.

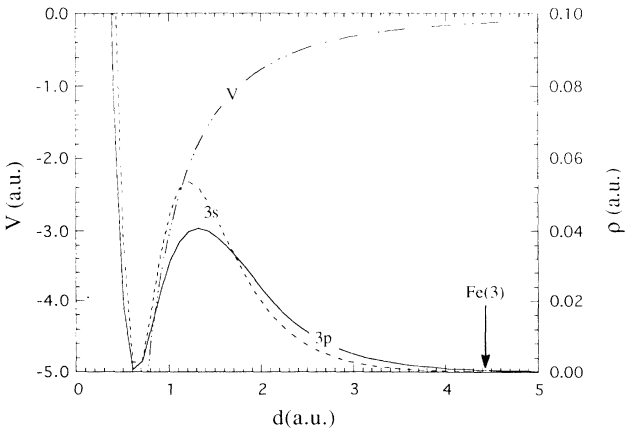

FIG. 4. The contributions of the 3s and 3p states to the valence charge density and total potential of the free phosphorus monolayer along the P-Fe(3) direction. Arrow denotes the position of the Fe(3) atom in the P/Fe Σ3[1$\bar{1}$0](111) GB.

Due to the short-range nature of the embedded interaction, the charge redistribution induced by the P impurity is mainly limited between P-Fe(1) and P-Fe(3) in both panels of Fig. 3. Therefore, the small cell with only the first rank of Fe neighbors is still useful for understanding the local chemical interaction.[5] As was found in our previous small-cell calculations, the P-induced Fe rehybridization weakens the Fe-Fe bonding as the charge density difference becomes negative in the regions between Fe(1)-Fe(2) and Fe(2) across the GB in Fig. 3(a), which might contribute to intergranular embrittlement as suggested by Briant and Messmer.[18]

Density-of-states (DOS) plots are shown in Fig. 5(a) for the P/FeΣ3[1$\bar{1}$0](111) GB and in Fig. 5(b) for P/Fe(111), where the solid curves denote majority spin

and dashed curves denote minority spin. In both cases, the Fe(7) atom shows bulk DOS behavior, indicating that the slab size effects are already reasonably small in the present models. Due to the low effective embedded potential from the Fe atoms, the P $3p$ states lie well below the Fe $3d$ band in the GB environment. Compared to the band centers with respect to E_F for the P monolayer, the P $3p$ band is lowered by 6 eV (from 0 to -6 eV) while the $3s$ band is lowered by 3.5 eV (from -8.5 to -12.0 eV). The lack of band overlap (except for some tail effects) indicates the weakness of the hybridization between P and Fe states. On the Fe(111) surface, by contrast, the higher potential on the vacuum side lifts the P $3p$ band up to the same energy range with the Fe $3d$ states. The shorter interatomic distance results in a stronger charge accumulation between P-Fe(3) in Fig. 3(b). However, from consideration of both the greater number of Fe neighbors and the lower energy of the P $3p$ band, P should be more energetically stable in the grain boundary environment from the pure chemical interaction point of view.

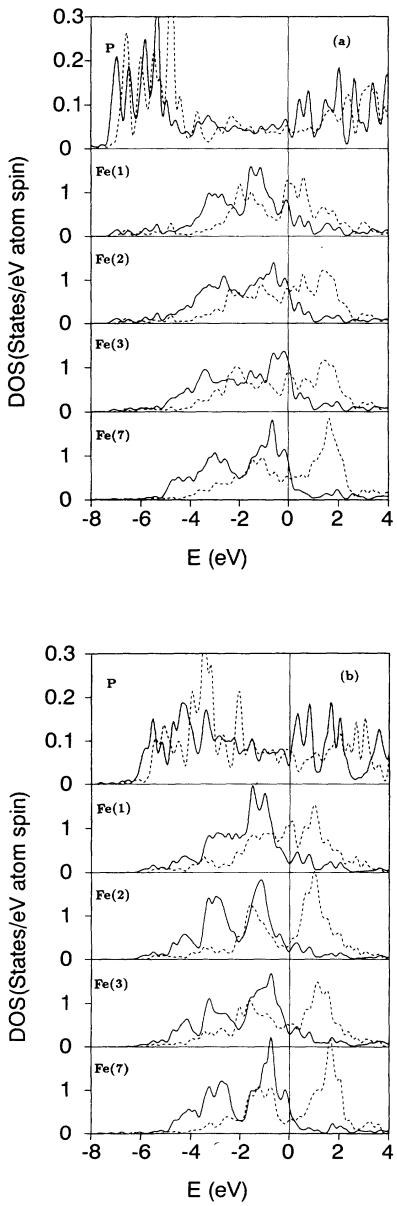

FIG. 5. The projected density of states (a) for the P/FeΣ3[1$\bar{1}$0] (111) grain boundary and (b) for the P/Fe(111) free surface. Solid (dashed) lines represent majority (minority) spin.

C. Magnetic interaction

Dramatically, unlike the antiferromagnetic coupling for the ω Fe phase, ferromagnetic coupling is restored in the P-segregated FeΣ3[1$\bar{1}$0](111) GB. In Fig. 5, a large exchange splitting can be found for each Fe atom. Even for P, the $3p$ band for majority spin separates from that for minority spin by 0.5 eV in both GB and FS environments.

As revealed in our previous small-cell calculation, P impurities strongly diminish the magnetization of their surrounding Fe atoms when GB relaxation is neglected. This is confirmed in the present calculation with larger cells. As shown in Fig. 6 by the spin density difference contours, the detrimental effects of P impurities on the magnetization around Fe(1), Fe(2), and Fe(3) are very clear. However, as was not revealed in the previous small-cell calculations, P induces an enhancement of magnetization around the second-rank Fe atoms. This behavior is not seen in the charge density difference of Fig. 3, indicating that P induces a short-range perturbation (screening) for the charge distribution but shows a long-range (oscillatory) behavior for the magnetic disturbance. Note that the spin density at the P site is very small, and so P does not carry a large magnetic moment ($\approx -0.01\mu_B$) although its $3p$ band exhibits some exchange splitting. By comparison, P shows stronger [weaker] effects on Fe(2) [Fe(3)] in the grain boundary than in the FS.

Quantitatively, as listed in Table I, the magnetic moment of Fe(1) is reduced by $1.0\mu_B$ (from $2.4\mu_B$ to $1.4\mu_B$), while the magnetic moments at Fe(2) and Fe(3) sites decrease only by $0.3\mu_B$ (to $1.81\mu_B$ and $1.49\mu_B$, respectively) compared to those for the unrelaxed GB1 case. Away from the first-rank Fe atoms, the effects of P impurities exhibit an oscillatory behavior until the Fe(9) site. For the P/Fe(111) FS, the P-induced change of magnetic moment also retains a distinct value ($0.2\mu_B$) at the center layer Fe(7), indicating a long-range behavior of the magnetic perturbation. Note that due to a shorter P-Fe(3) distance, the effects of the P impurity on the Fe(3) [Fe(2)] are enhanced [reduced] for P/Fe(111) compared to those in the P/FeΣ3[1$\bar{1}$0](111) GB.

However, since the magnetic moments are frustrated by the antiferromagnetic coupling and shorter interatomic distance [especially for Fe(5); cf. the column for GB0 in Table I] in the ω phase of the relaxed clean GB, the P impurity enhances the magnetization for almost all Fe atoms if the effects of structural relaxation are included. The large variance of the magnetic moment is expected to contribute to the total energy and thus affect the cohesive properties. The greater P-induced magnetic moment increase in the GB compared to the surface suggests a magnetic contribution that reduces the embrittling potency of P in Fe.

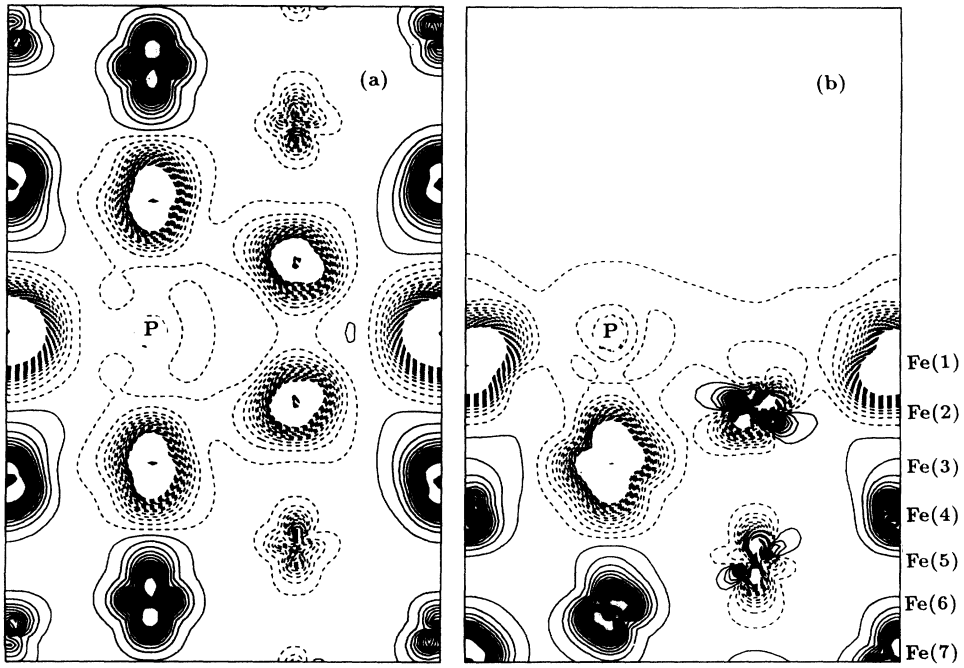

FIG. 6. The P-induced spin density difference for (a) the P/FeΣ3[1$\bar{1}$0] (111) grain boundary and (b) the P/Fe(111) free surface. Dashed lines show negative differences.

V. SEGREGATION ENERGY

The calculated segregation energies (defined as $\Delta E = E_{P/Fe} - E_{Fe} - E_P$ with E the total energy for each system) for a P impurity in the Fe GB and on the Fe(111) surface and their differences are listed in Table II. Results are listed for the "chemical" interactions without structural relaxation, the "mechanical" interaction represented by structural relaxation of the clean Fe GB and FS, and the sum of these contributions defines the total interaction energy. Note that by including the P-induced structural relaxation, the segregation energy in the grain boundary environment is smaller (less negative) than that on the FS, i.e., $\Delta E_b^0 - \Delta E_s^0 = 0.79$ eV > 0, in good agreement with the experimental value (0.4±0.2 eV/P atom). According to Rice and Wang's thermodynamic theory,[2] P is thus an embrittler for the cohesion across the Fe GB.

As before, $\Delta E_b^0 - \Delta E_s^0 = -0.75$ eV < 0 is obtained if the elastic energy released from the clean FeΣ3[1$\bar{1}$0](111) GB is excluded. This elastic energy, as seen from Table II, is as large as 1.61 eV/cell (2.19 eV/cell for the nonmagnetic case) which overwhelms the chemical energy difference −0.75 eV. By contrast, the atomic relaxation on the clean surface has only a minimal contribution (< 0.1 eV/cell) to ΔE_s^0. Therefore, the more favorable chemical interaction of P in the GB environment is more than compensated by the elastic energy penalty of accommodating P in the GB environment, favoring greater stability in the FS environment and hence an embrittling effect.

From Table II, we can see that the magnetic energies are not very important for either ΔE_b^0 or ΔE_s^0 separately, but are indeed very important for their difference. As indicated in Table I, P diminishes the magnetization for the surrounding Fe atoms, and thus is expected to reduce the binding energy. This is the case on the FS where the spin-polarized calculations result in a ΔE_s^0 value about 0.2 eV/cell smaller (less negative) than the corresponding results from nonmagnetic calculations. However, due to

TABLE II. Calculated segregation energies (in eV) for the P/FeΣ3[1$\bar{1}$0](111) GB and the P/Fe(111) FS for ferromagnetic (FM) and nonmagnetic (NM) states.

	ΔE_b	ΔE_s	$\Delta E_b - \Delta E_s$	ΔE_M
Unrelaxed (chemical)				
NM	−8.16	−7.58	−0.58	
FM	−8.19	−7.44	−0.75	−0.17
Relaxation (mechanical)				
NM	2.19	0.01	+2.18	
FM	1.61	0.07	+1.54	−0.64
Relaxed (total)				
NM	−5.97	−7.57	+1.60	
FM	−6.58	−7.37	+0.79	−0.81

the complexity in the GB, the contribution of the magnetization to ΔE_b^0 seems very small for the unrelaxed case. Using the ω Fe as the reference system, however, the magnetization even enhances the binding energy since the larger local magnetic moments and the ferromagnetic coupling are energetically more favorable for Fe. The magnetic increment ΔE_M to the GB-FS segregation energy differences listed in Table II shows that the net effect of magnetism is to reduce the embrittling potency of P in Fe.

From the above discussion, we know that P and Fe interact mainly via an effective embedded potential instead of covalent bonding. This mechanism can be easily extended to other $3p$ metalloid impurities in Fe grain boundaries. By contrast, since there is no node for the $2p$ radial wave function, $2p$ impurities (such as B) are expected to interact with surrounding Fe atoms via covalent hybridizations.[7] In this sense, the embrittlement properties for $2p$ and $3p$ metalloids may differ significantly, but similar behaviors are expected for each set. Calculations for the C/FeΣ3[1$\bar{1}$0](111) GB and S/FeΣ3[1$\bar{1}$0](111) GB are underway to test this hypothesis which appears supported by available experimental data. The mechanism of the embedded atom behavior was also used by Cottrell[19] to explain the different embrittlement properties for H and O vs B, C, and N. He concluded that the covalent elements (B, C, and N, with their $2p$ bands floating at E_F) enhance while embedded elements (H and O, with their valence band sunk to the bottom of the d band) weaken the cohesion of the Fe grain boundary. Our calculations offer some support for this concept, but we find that large binding energies can also be obtained from embedded attraction.

VI. CONCLUSION

In conclusion, we have obtained the segregation energies for P impurities on the Fe(111) FS and in the FeΣ3[1$\bar{1}$0](111) GB on an equal footing using state-of-the-art FLAPW energy band calculations based on a slab model. The clean FeΣ3[1$\bar{1}$0](111) GB is found to undergo an ω phase transition with an AFM coupling. This relaxation, in turn, makes a key contribution to the segregation energy ΔE_b, which is crucial for the final energy difference $\Delta E_b - \Delta E_s$ and thus the embrittlement properties. Interestingly, the P-Fe interaction is found to be more embedded atom like instead of a covalent hybridization due the large separation of the P $3p$ wave function from its nucleus. Magnetic contributions somewhat reduce the embrittlement potency of P in Fe. The nature of observed bonding offers some insight into the role of other solutes in the cohesion of the Fe grain boundary.

ACKNOWLEDGMENTS

This work was supported by the Office of Naval Research (Grant No. N00014-90-J-1363) and a grant for computer time at the NSF Pittsburgh Supercomputing Center Cray-C90 supported by its Division of Advanced Scientific Computing.

[1] G.B. Olson, in *Innovations in Ultrahigh-strength Steel Technology*, edited by G.B. Olson, M. Azrin, and E.S. Wright, 34th Sagamore Army Materials Research Conference Proceedings (U.S. Army Laboratory Command, 1990), p. 3.
[2] J.R. Rice and J.-S. Wang, Mater. Sci. Eng. A **107**, 23 (1989).
[3] P.M. Anderson, J.-S. Wang, and J.R. Rice, in *Innovations in Ultrahigh-strength Steel Technology*, edited by G.B. Olson, M. Azrin, and E.S. Wright, 34th Sagamore Army Materials Research Conference Proceedings (U.S. Army Laboratory Command, 1990), p. 619.
[4] J.-S. Wang and J.R. Rice (unpublished).
[5] R. Wu, A.J. Freeman, and G.B. Olson, J. Mater. Res. **7**, 2433 (1992).
[6] S.P. Tang, A.J. Freeman, and G.B. Olson, Phys. Rev. B **47**, 2441 (1993).
[7] R. Wu, A.J. Freeman, and G.B. Olson, Phys. Rev. B **47**, 6855 (1993).
[8] G.L. Krasko and G.B. Olson, Solid State Commun. **76**, 247 (1990).
[9] R. Wu and A.J. Freeman, Phys. Rev. B **47**, 3904 (1993).
[10] E. Wimmer, H. Krakauer, M. Weinert, and A.J. Freeman, Phys. Rev. B **24**, 864 (1981), and references therein.
[11] D.D. Koelling and B.N. Harmon, J. Phys. C **10**, 3107 (1977).
[12] U. von Barth and L. Hedin, J. Phys. C **5**, 1629 (1972).
[13] A.J. Freeman and R. Wu, J. Magn. Magn. Mater. **100**, 497 (1992).
[14] R. Wu and A.J. Freeman, Comput. Phys. Commun. **76**, 58 (1993).
[15] G.L. Krasko, in *Structure and Properties of Interfaces in Materials*, edited by W. A. T. Clark, U. Dahmen, and C. L. Briant, MRS Symposia Proceedings No. 238 (MRS, Pittsburgh, 1991), p. 481.
[16] B. Aronsson and S. Rundquist, Acta. Crystallogr. **15**, 878 (1962); S. Rundquist, Ark. Kemi **20**, 67 (1962).
[17] J. Sokolov, F. Jona, and P.M. Marcus, Phys. Rev. B **33**, 1397 (1986).
[18] C.L. Briant and R.P. Messmer, Philos. Mag. B **42**, 569 (1980).
[19] A.H. Cottrell, Mater. Sci. Technol. **6**, 807 (1990).

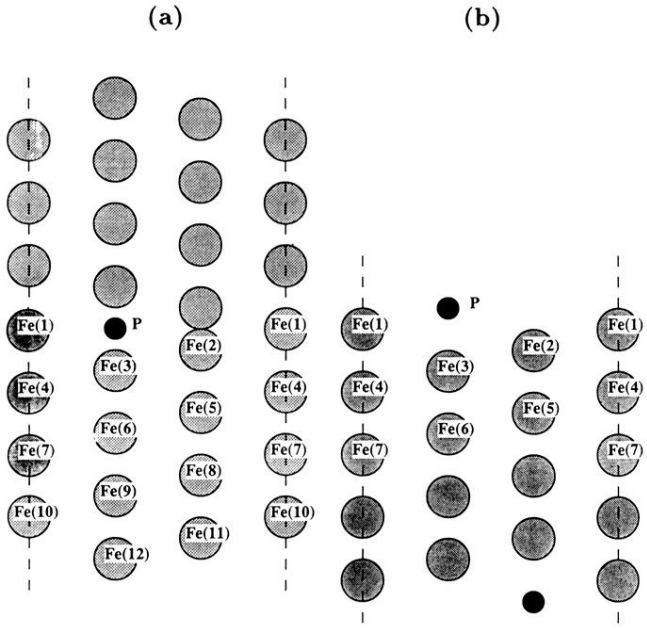

FIG. 1. Model and notation for the structure of (a) the P/Fe $\Sigma 3[1\bar{1}0](111)$ "incoherent" twin boundary and (b) the P/Fe(111) surface.